Preliminary Testing of a Passive Exoskeleton Prototype Based on McKibben Muscles

machines

MDPI

Article

Preliminary Testing of a Passive Exoskeleton Prototype Based on McKibben Muscles

Maria Paterna, Carlo De Benedictis * and Carlo Ferraresi

Department of Mechanical and Aerospace Engineering, Politecnico di Torino, 10129 Turin, Italy; maria.paterna@polito.it (M.P.); carlo.ferraresi@polito.it (C.F.)
* Correspondence: carlo.debenedictis@polito.it

Abstract: Upper-limb exoskeletons for industrial applications can enhance the comfort and productivity of workers by reducing muscle activity and intra-articular forces during overhead work. Current devices typically employ a spring-based mechanism to balance the gravitational torque acting on the shoulder. As an alternative, this paper presents the design of a passive upper-limb exoskeleton based on McKibben artificial muscles. The interaction forces between the exoskeleton and the user, as well as the mechanical resistance of the exoskeleton structure, were investigated to finalize the design of the device prior to its prototyping. Details are provided about the solutions adopted to assemble, wear, and regulate the exoskeleton's structure. The first version of the device weighing about 5.5 kg was manufactured and tested by two users in a motion analysis laboratory. The results of this study highlight that the exoskeleton can effectively reduce the activation level of shoulder muscles without affecting the lumbar strain.

Keywords: passive exoskeleton; pneumatic artificial muscles; industrial exoskeleton; McKibben; contact pressures; FEM; soft actuators; worker assistance; arm support; EMG

check for updates

Citation: Paterna, M.; De Benedictis, C.; Ferraresi, C. Preliminary Testing of a Passive Exoskeleton Prototype Based on McKibben Muscles. *Machines* **2024**, *12*, 388. https://doi.org/10.3390/machines12060388

Academic Editor: Dan Zhang

Received: 24 April 2024
Revised: 31 May 2024
Accepted: 3 June 2024
Published: 5 June 2024

1. Introduction

Wearable upper-limb exoskeletons have been proposed to improve worker ergonomics by performing repetitive or physically demanding tasks. Exoskeletons allow workers to handle heavier weights and avoid excessive muscle fatigue by applying pressure on the human body. Based on the working principle, exoskeletons can be classified as active or passive. In the first case, one or more actuators are integrated into the structure to provide the power source required to complete the movement [1–4]. By contrast, the second type employs passive elastic mechanisms to counteract the gravitational torque on the joints [5–7].

Regardless of the exoskeleton type, the close physical human–robot interaction imposes several requirements and constraints in the exoskeleton design process. The forces applied by the exoskeleton on the user must be below the pain detection threshold (PDT, i.e., the pressure level beyond which the pain occurs) to avoid damage to soft tissues. Although the high inter-subject variability makes it hard to define a standard PDT value, recent findings indicate that the maximum pressures should not exceed 6 kPa for the trunk [8], 15 kPa for the pelvis [8], and 30 kPa for the upper arm [9]. In addition, an exoskeleton must ensure a range of motion sufficient to perform working activities while maintaining a light and compact structure to avoid increasing the effort of the lumbar muscles and cardiovascular demands or worsening balance performance [10,11]. Moreover, the assistive torque profile should be easily adjustable as the load on the shoulder depends on the weight of the upper limb and any tool held by the user, as well as the working task. Finally, exoskeletons should be simple to wear and adjust to different user physical characteristics (e.g., shoulder width or waist height). Exoskeletons should not negatively hinder human mobility because quick and complex movements may be required in industrial environments to preserve worker productivity and safety.

The metric most commonly used to assess the effectiveness of the exoskeletons in assisting workers is the assessment of electromyographic activity of the shoulder muscles during experiments in which typical working tasks, such as light assembly, overhead drilling, wiring, or painting, are simulated [12–15]. Improvements in the accuracy and speed of work tasks have also been reported as effectiveness indicators. Task performance metrics depend on the specific task and include onset fatigue time [16,17], number of errors [10], number of repetitions during a time period [16], and execution time [10,16,18,19]. On the other hand, alterations in the arm kinematics and balance performances, or increases in the efforts of unassisted muscles, were investigated to verify the potential undesired effects of the exoskeleton [10,11,20]. Finally, several studies provided subjective ratings of some devices, using acceptability [4,5,10,16,21] and usability [21] questionnaires.

This study presents the design and development of an exoskeleton with a compact and straightforward shoulder linkage structure and sufficient range of motion (ROM) to perform overhead working tasks. The assistive mechanism passively generates the assistive torque about the shoulder joint through a pressurized McKibben muscle (MKM) and a transmission based on a wire that wraps on an appropriately conceived shoulder pad. MKMs are advantageous for several reasons. They do not significantly affect the device's weight or overall size because of their high power-to-weight ratio and ease of installation. Their softness and similarity to human skeleton muscles further promote safe human–exoskeleton interaction. Their supply pressure may also be changed to modulate the action level and customize the exoskeleton action to the working task requirements. Lastly, MKMs may find usage in industrial applications because they are inexpensive and resilient to high temperatures, thermal gradients, dusty conditions, and unclean surroundings. Despite this, MKMs are not widespread because the high footprint of their energy source relegates their use in fixed workstations. However, MKMs can be integrated into the exoskeleton structure as passive elements to overcome this issue. The MKM is energized at the beginning of the working activity, and then, the pressure is maintained constant throughout the working cycle. The assistance level can be easily adjusted by manually changing the supply pressure before or during usage. By design, the system is able to exert a supporting torque for different arm elevation angles, which correspond to different MKM shortening or contraction. The match between the support and the gravitational torques throughout the shoulder flexion range of movement is guaranteed by the shoulder pad profile. The latter was designed to ensure an MKM lever arm that increases as the elevation angle increases. In this way, the mismatch between the gravitational and support torques is reduced as much as possible in a range of flexion angles ranging from 90° to 135°.

More details on the design of the shoulder pad are provided in previous works of the authors [22,23]. The focus of the current paper is the presentation of the final architecture of the first prototype of the exoskeleton. For this purpose, the paper deals with details related to the mechanical structure of the device, the actual implementation, and the experimental validation of the proposed solution. To the authors' knowledge, no previous study attempted to integrate an MKM as a passive element into an upper-limb exoskeleton. The rest of this article is organized as follows: In Section 2, the exoskeleton architecture is presented. Section 3 describes the analytical model used for the estimation of human–exoskeleton interaction forces, the finite element static analysis, and the experimental laboratory test protocol designed to validate the exoskeleton's effectiveness. The analytical, numerical, and experimental results are presented and discussed in Section 4 Finally, Section 5 concludes this article.

2. Exoskeleton Architecture

The exoskeleton is designed to maximize the support torque in a sufficiently wide working range without causing the onset of high human–exoskeleton interaction forces. The exoskeleton structure consists of two exo-arms, a back frame, and a commercial harness. In what follows, the numbering in brackets refers to the elements shown in Figure 1. The support

torque is generated by two McKibben muscles (DMSP-10-350N-RM-CM, FESTO, Esslingen am Neckar, Germany), (1) one for each arm, placed behind the back of the user. An L-shaped plate secures MKM's top ends to the fixed back-frame upper beam, while the lower ends are attached to a wire (Braided climax-200daN, OCKERT, Puchheim, Germany) via a custom eye rod. A high-density polyethylene-coated steel sheath and two sheath clamps enable the wire to reverse its direction, before it wraps over the shoulder pad (2) and connects to the bracelet (3) that supports the upper arm. The shoulder pad profile is designed to modulate the MKM traction force lever arm according to the shoulder flexion angle in order to adapt the support torque to the gravitational torque acting on the shoulder [22,23]. The bracelet, whose inner surface is covered with a polyamide coating, is fastened to a strut (4) to prevent it from sliding due to the MKM action. Several bracelet positions are arranged to fit the user's upper arm length. The strut articulates with a horizontal axis hinge (5), which is in turn coupled to a vertical axis hinge (6). The two hinges' axes converge on the ideal center of the shoulder joint (SJC). Their combination allows for shoulder flexion and abduction between 90° and 135° and between 0° and 30°, respectively. The bracelet, the two hinges, and the shoulder pad constitute the exo-arm, which is rigidly clamped (KPVV 10, RS Rose+Krieger, Minden, Germany) (7) to the back frame.

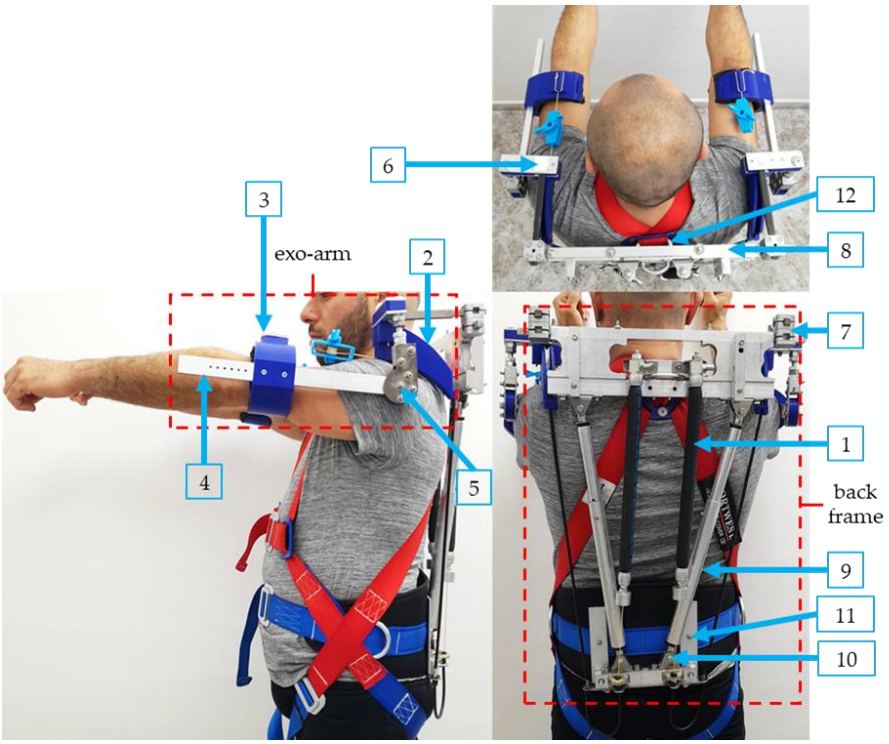

Figure 1. Exoskeleton architecture.

The exoskeleton performance is dependent on the exoskeleton and anatomical joints' axes alignment. Therefore, adjustable elements are included in the back frame to adjust the joint axes' location to the user's shoulder width and shoulder–pelvis distance. The vertical hinges' axes are aligned to the shoulder abduction axes thanks to a square telescopic bar (8), while the horizontal hinges' axes are aligned to the shoulder flexion axes through two telescopic rods (9). To guarantee the user's trunk's free movement, four additional hinges (10), two for each rod, allow for the rotation of the telescopic rods on the frontal plane.

Finally, the exoskeleton is worn thanks to a 3 D-Rings commercial harness (FP14–Portwest, Thurnscoe, UK) for suspension. The pelvic belt (11) of the harness is bolted to the back-frame lower beam, while the dorsal D-ring (12) is clamped to the exoskeleton via a custom-made grip conforming to the ring shape.

The prototype is designed for users with heights ranging from 160 cm to 175 cm. The distance between the bracelet and the horizontal hinge can be adjusted from 18 cm to 26 cm, the shoulder width from 37 cm to 41 cm, and the shoulder–pelvis distance from 46 cm to 50 cm. Finally, to increase user comfort, a polyamide coating is applied to the inside surface of the bracelets and the bottom of the shoulder pads.

3. Methods

3.1. Simulation Analysis

The safety and ergonomics of exoskeletons can be assessed preliminarily by structural stress analysis and model simulations. In particular, human–exoskeleton interaction forces can be estimated by an analytical approach, that is by solving the static equilibrium of the system and by knowledge of contact areas between the human body and the mechanical structure. The entity of contact pressures indeed plays a significant role in the usability of the exoskeleton, especially for long-lasting working activities. The bracelets, pelvic belt, and thoracic belt are the user's points of contact with the exoskeleton. The user's body pressures at these sites can be estimated for different shoulder joint angles, that is, by exploiting the entire workspace of the exoskeleton.

The weight of the arm and any tools used by the user, as well as the user's muscular action, all contribute to the bracelet–arm contact force (F_a). It is possible to determine the gravitational force (F_w) by approximating the user's arm to a rigid link with mass centered in its center of mass, hinged in SJC, and supported by a roller at the bracelet (Equation (1)).

$$F_w = \frac{M_g}{l \cdot \sin(\theta_f)} \tag{1}$$

In Equation (1), M_g is the gravitational torque at the shoulder, l is the distance between SJC and the middle of the bracelet (Figure 2), and θ_f is the shoulder flexion angle measured relative to the resting position (arms aligned to the trunk).

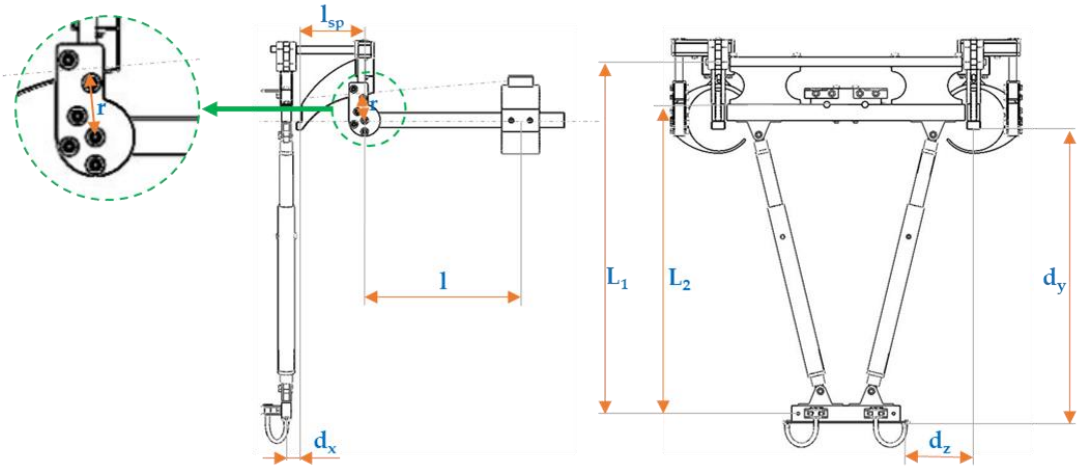

Figure 2. Geometrical parameters of the exoskeleton model.

On the other hand, the amount of muscular effort (F_m) required to maintain the ideal arm posture is determined by two contributions. The first is the muscular force required to correct for the mismatch between gravity and exoskeleton support torque (F'_m) in order to maintain the appropriate flexion angle (θ_f). The second contribution is the effort (F''_m) required to maintain the ideal abduction angle (θ_a). Referring to the geometrical parameters and the exo-arm model shown, respectively, in Figures 2 and 3a, Equations (2)–(8) may be used to evaluate F'_m and F''_m.

$$F'_m = \frac{F_{MKM} \cdot r - F_w \cdot l \cdot \sin(\theta_f)}{l} \tag{2}$$

$$F''_m = \frac{F'_m \cdot \cos(\theta_f) \cdot \cos(\theta_a) \cdot b_1 + F_{MKM} \cdot \sin(\alpha) \cdot \sin(\beta) \cdot b_2 - F_{MKM} \cdot \sin(\alpha) \cdot \sin(\beta) \cdot b_3}{(l \cdot \sin(\theta_f) + r_b \cos(\theta_f)) \cdot \cos(\theta_a)} \tag{3}$$

$$b_1 = (l \cdot \cos(\theta_f) + r_b \sin(\theta_f)) \cdot \sin(\theta_a) \tag{4}$$

$$b_2 = l_{sp} \cdot \sin(\theta_a) \tag{5}$$

$$b_3 = l_{sp} \cdot \cos(\theta_a) \tag{6}$$

$$\alpha = \operatorname{acos}\left(\frac{d_y}{\sqrt{d_x^2 + d_y^2 + d_z^2}}\right) \tag{7}$$

$$\beta = \operatorname{acos}\left(\frac{d_x}{d_z}\right) \tag{8}$$

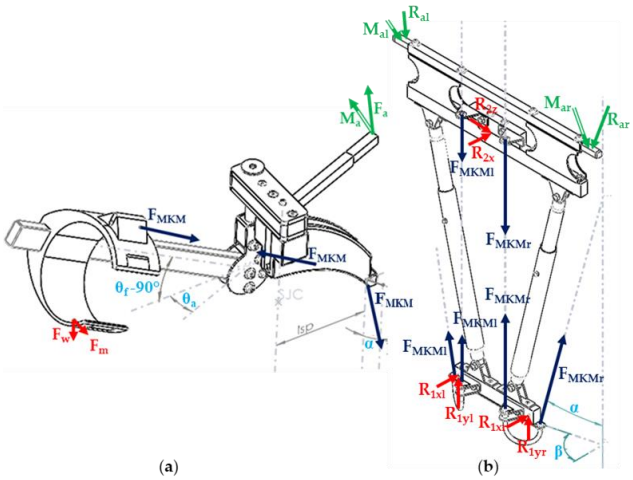

Figure 3. A 3D scheme of the forces acting on the (**a**) exo-arm and (**b**) back frame.

In Equations (2)–(8), r is the distance between the horizontal hinge axis and the MKM tensile force applied on the bracelet. In other words, r is the exoskeleton support torque lever arm; l is the distance between the middle of the bracelet and the horizontal axis hinge; b_1 is the lever arm of the anteroposterior component of F'_m with respect to the vertical hinge axis; b_2 is the lever arm of the anteroposterior component of F_{MKM} applied on the shoulder pad rear part with respect to the vertical hinge axis; b_3 is the lever arm of the craniocaudal component of F_{MKM} applied on the shoulder pad rear part with respect to the vertical hinge axis; r_b is the bracelet inner radius; l_{sp} is the horizontal shoulder pad length; α is the angle between the wire and craniocaudal axis calculated on the plane that contains both the wire and the craniocaudal axis (see Figure 3); β is the angle between the projection of F_{MKM} on the transverse plane and anteroposterior axis (see Figure 3); and d_x, d_y, and d_z are the components of the distance between the rear of the shoulder pad and sheath clip.

Finally, F_a can be obtained as follows:

$$F_a = \sqrt{(F'_m \cdot \cos(\theta_f) \cdot \cos(\theta_a))^2 + (F'_m \cdot \sin(\theta_f) + F_w)^2 + \left(F''_m\right)^2} \tag{9}$$

The static equilibrium of the back frame, shown in Figure 3b, can be solved using Equations (10)–(13):

$$R_{1x} = R_{1xr} + R_{1xl} = R_{axr} + R_{axl} - R_{2x} - \left(F_{MKM_r} + F_{MKM_l}\right) \cdot \sin(\alpha) \cdot \cos(\beta) \tag{10}$$

$$R_{2x} = \frac{\left(R_{ax_r} + R_{ax_l}\right)\cdot L_1 - M_{ax_r} - M_{ax_l}}{L_2} \tag{11}$$

$$R_{1y} = R_{1y_r} + R_{1y_l} = R_{ay_r} + R_{ay_l} - \left(F_{MKM_r} + F_{MKM_l}\right)\cdot\cos(\alpha) \tag{12}$$

$$R_{2z} = R_{az_r} - R_{az_l} + \left(F_{MKM_l} - F_{MKM_r}\right)\cdot\sin(\alpha)\cdot\sin(\beta) \tag{13}$$

In Equations (10)–(13) R_1 is the reaction force on the pelvic belt; R_a and M_a are the reaction force and torque exerted by the back frame on the exo-arm and can be obtained by solving the static equilibrium of the exo-arm illustrated in Figure 3a; R_2 is the thorax belt reaction force; L_1 is the back-frame height; L_2 is the distance between the dorsal exoskeleton–harness connection and the pelvis fixing point; and F_{MKM} is the MKM traction force. The subscripts x, y, and z refer to the anteroposterior, craniocaudal, or mediolateral component of the forces, while subscripts r and l refer to the right and left sides.

Finally, the forces applied on the thorax (F_t) and pelvis (F_p) can be calculated (Equations (14) and (15)).

$$F_t = R_{2x} \tag{14}$$

$$F_p = \sqrt{R_{1x}^2 + R_{1y}^2 + R_{2z}^2} \tag{15}$$

The simulations were performed considering an average height man (70 kg, 1.7 m) in the heaviest working condition (extended elbows and a 2 kg tool in the right hand). The gravitational torque was calculated based on the anthropometric parameters reported by Winter [24], while the assistive torque was obtained using the model described in [22,23] assuming an MKM supply pressure equal to 4.3 bar and 7.7 bar, for the left and right arm, respectively.

As stated at the beginning of this section, another important aspect to determine in order to have preliminary information about safety during the exoskeleton design is the load resistance of the exoskeleton's rigid structure. To this end, the Simulation tool of SolidWorks® (2023) was used to perform a static stress structural analysis through the finite element method (FEM). The same constraints established for the interaction force model were used (see Figure 4), while the loads replicated the most demanding working condition ($\theta_f = 90°$; $\theta_a = 0°$; fully extended elbows; a 2 kg tool in the right hand). In particular, the bracelet was subjected to the MKM traction force (F_{MKM}) and also to a downward force F_a that simulated the overall force resulting from gravitational load and muscular force required to maintain the appropriate flexion angle of 90° and the abduction angle of 0°. F_{MKM} was also applied on the shoulder pad profile and the top of the back frame. By contrast, the wire traction forces ($F'_{w\text{ire}}$, $F''_{w\text{ire}}$) were applied on its lower part. Finally, the gravitational load due to the weight of the exo-arm (F_{w1}) and the weight of the back frame (F_{w2}) were applied to the respective centers of gravity.

The materials used in the simulation were stainless steel (DIN 1.4301, X5CrNi18-10) for fixed hinge elements, the square telescopic bars, and support plates of both MKMs and sheath clamps; PLA for the peculiar-shaped components (in turquoise in Figure 4); and aluminum alloy (EN AW–6060–t6) for all other components. The mechanical characteristics of the selected materials are listed in Table 1.

Table 1. Young's modulus (E), Poisson's ratio (v), shear modulus (G), yield strength (S_y), and ultimate strength (S_{ut}) of the selected materials.

Material	E (MPa)	v	G (MPa)	S_y (MPa)	S_{ut} (MPa)
DIN 1.4301 (X5CrNi18-10)	200,000	0.28	79,000	400	600
EN AW–6060-t6	66,000	0.33	25,000	230	230
PLA (printing direction)	2904.2	0.292	723.34	56	56
PLA (other directions)	2597.5	0.299	1010	35	35

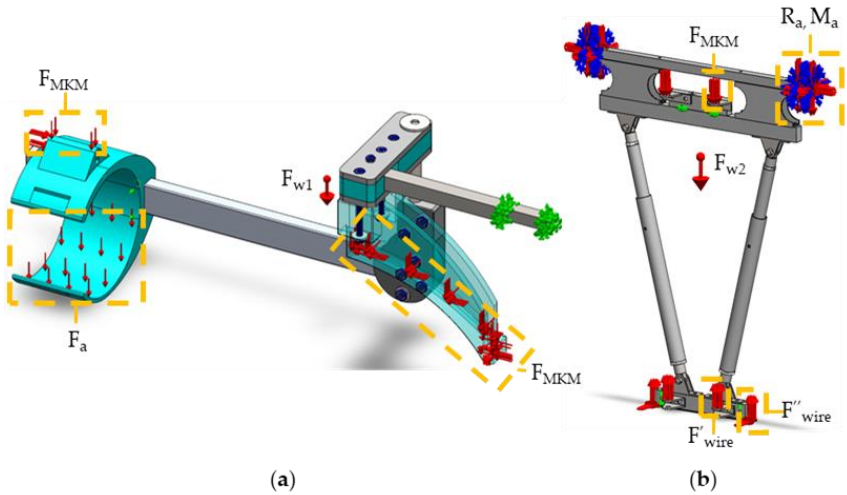

Figure 4. FEM analysis boundary condition: (**a**) exo-arm; (**b**) back frame.

3.2. Experimental Validation

Two healthy subjects (one male and one female), whose anthropometric measurements are listed in Table 2, were involved in the experimental tests. Both volunteers were right-handed and had never worn an exoskeleton before. Subjects were asked to complete both static and dynamic tasks.

Table 2. Subjects' anthropometric characteristics.

Subject	Gender	Height (m)	Weight (kg)	Age (Years)
1	F	1.72	80	31
2	M	1.60	67	34

Static tasks required the subject to stand upright, with both arms flexed at a 90° angle while holding a power drill (weighing 1.2 kg) in the right hand. The elbows should be fully extended, but a slight flexion was allowed to make the user comfortable. To help the participants keep their arms in the defined position, a reference point was drawn on a panel in front of them.

On the other hand, dynamic tasks required participants to stand up and trace the contour of a rectangle (b = 20 cm; h = 30 cm) on a panel in front of them with their right hand. The task was repeated while holding a portable tool. To ensure that the shoulder flexion angle ranged between 90° and 110°, the panel height was adjusted according to the subject height. The elbow was in the most extended position, which was still comfortable for the user. Subjects were asked to repeat the exercises 10 times at their own speed and to flex their elbow before each repetition to ease the subsequent segmentation of the signals.

The two subjects were asked to complete all tasks both wearing the exoskeleton (EXO session) and without the exoskeleton (FREE session). The order of FREE and EXO sessions was randomized among participants. An inter-task break of at least 5 min was allowed for rest. Owing to the aforementioned adjustable systems, the exoskeleton structure was modified to match the subjects' dimensions before the beginning of the EXO sessions, while the assistive level was adjusted to completely counterbalance the gravitational torque at a 90° shoulder flexion angle. The MKM-supply pressures were set to 6.5 bar and 4.5 bar on the right and left sides, respectively, given that only the right side was subjected to the tool weight.

During all tasks, the activity of two shoulder muscles (anterior and middle deltoid) and two lumbar muscles (longissimus and iliocostalis) were monitored using a wireless multichannel surface electromyographic system (Wave Plus, Cometa, Bareggio, Italy). Surface EMG pre-gelled, bipolar electrodes (silver-silver chloride electrodes, 24 mm, GEA soluzioni, Turin, Italy) were placed bilaterally over the shoulder and low-back muscles

following the SENIAM recommendations [25]. The skin was shaved and cleaned with alcohol before applying the electrodes to ensure better adhesion. Finally, the electrodes' placement correctness was checked using a real-time graphical user interface. EMG data were sampled at 1000 Hz and post-processed with a customized script in MATLAB 2022b (MathWorks Inc., Natick, MA, USA). Raw EMG signals were high-pass-filtered (4th Butterworth filter with 10 Hz cut-off frequency) and low-pass-filtered (4th Butterworth filter with 450 Hz cut-off frequency) to remove high-frequency noise and movement artifact. Then, EMG signals were rectified, and the average rectified value (ARV) was calculated.

Shoulder and elbow kinematics were also monitored using a twelve-camera optical motion capture system (Vicon Nexus). A modified plug-in-gait (PiG) model was implemented to track the body segments' orientation. Four reflective markers (diameter = 14 mm) were placed on the torso landmarks: the processus spinosus of the seventh cervical vertebra (C7) and of the tenth thorax vertebra (T10), the xiphoid process of the sternum (STRN), and the suprasternal notch (CLAV). Moreover, six reflective markers were placed on right and left landmarks: the acromion clavicular joint (SHO), the clavicular bone (CLA) halfway between the SHO and CLAV, the lateral (ELB) and medial (ELBM) epicondyles of the humerus, and the medial (WRA) and lateral (WRB) sides of the wrist. In addition, a marker was placed anywhere over the right forearm (RFA) to facilitate automatic marker labeling. The complete marker set is shown in Figure 5.

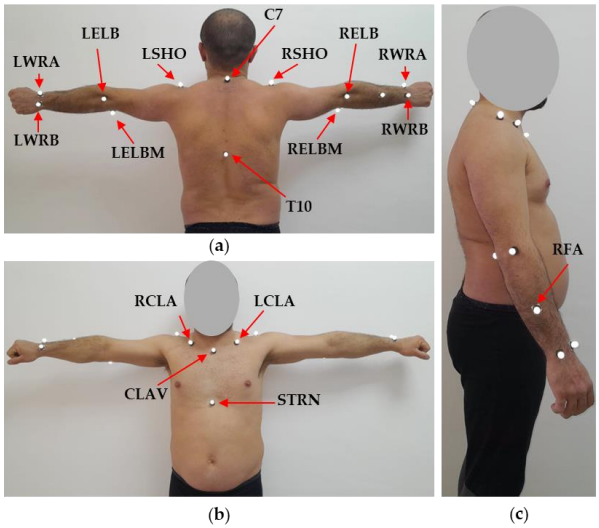

Figure 5. (**a**) Back, (**b**) front, and (**c**) right side view of the marker set.

Marker trajectories were sampled at 100 Hz. Raw trajectory data were low-pass-filtered (4th Butterworth filter with 6 Hz cut-off frequency) to remove movement and reconstruction artifacts. The flexion–extension angle of both the shoulder and elbow and the abduction–adduction angle of the shoulder were estimated from marker trajectories using a custom-made MATLAB script.

Finally, the coordinates on the transverse plane of the center of the pressures exchanged between foot and ground (CoP) were provided using the force platform (BMS400600, AMTI, Watertown, MA, USA). The CoP displacement in the anteroposterior and mediolateral directions was sampled at 1000 Hz and passed through a fourth-order zero-phase Butterworth low-pass digital filter with a 20 Hz cut-off frequency. The RMS amplitude of the CoP displacement in the transverse plane (CoP_{rms}) was then calculated.

An example of the signals acquired during the experimental tests is given in Figure 6. The performance metrics (ARV, CoP_{rms}, shoulder flexion, and abduction angles) were calculated using two distinct approaches depending on the experimental task type. In static tasks (Figure 6a), performance parameters were determined within the final 50 s of acquisition,

whereas for dynamic tasks (Figure 6b), performance parameters were calculated for each of the 10 repetitions and then averaged to provide a single index for each dynamic task.

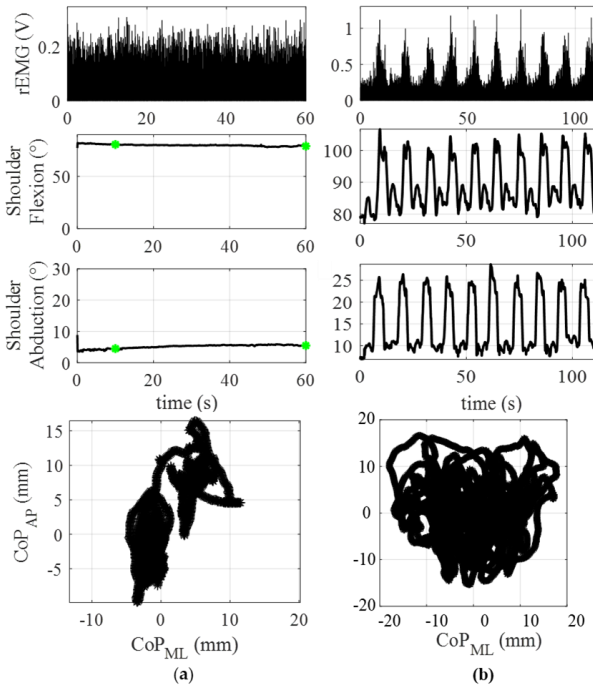

Figure 6. A representative recording of the acquired signals in (**a**) static and (**b**) dynamic tasks.

4. Results and Discussion

4.1. Simulation Results

The human–exoskeleton interaction forces, expressed by Equations (9), (14), and (15), were used to calculate the pressures applied on the upper arm (Figure 7a), the thorax (Figure 7b), and the pelvis (Figure 7c) of the user in the exoskeleton working range, that is, by varying the shoulder flexion angle (x-axis) and considering different abduction angles (as reported in the legend). The contact surfaces considered for each body area are, respectively, half of the inner surface of the bracelet, the chest belt, and the pelvic belt surfaces. It can be noticed that the pressures applied by the exoskeleton on the different body areas are lower than the respective pain detection thresholds (PDTs) [8,9] throughout the entire working range. These results are encouraging in terms of safety and comfort. Even with prolonged exoskeleton usage, the low contact pressures reduce the possibility of soft tissue injury to the user [8].

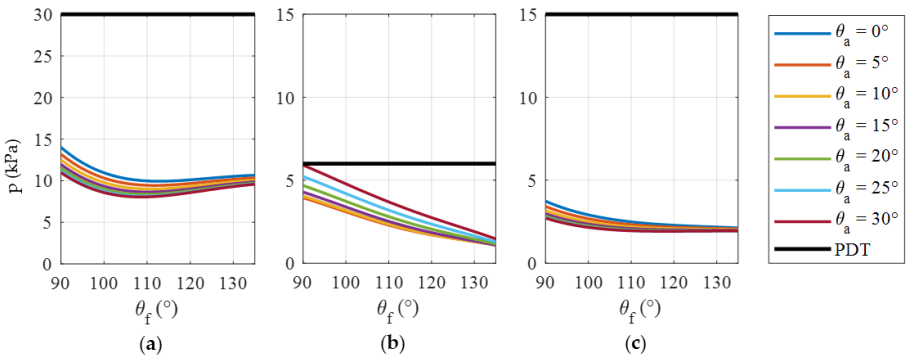

Figure 7. Contact pressures vs shoulder flexion angle on the (**a**) upper arm, (**b**) chest, and (**c**) pelvis, by selecting different abduction angles. The black lines represent the pain detection thresholds for each body area.

Regarding the mechanical stress analysis, in all back frame components, the maximum stresses are lower than the yield stress (Figure 8). The horizontal hinge's axis lowers by about 2 mm and shifts posteriorly by about 5 mm because of the applied loads (Figure 9a). Therefore, an offset between the exoskeleton and shoulder flexion axis must be considered while wearing the exoskeleton to avoid joint misalignment during the working activity. The bracelet is also lowered, reducing the shoulder flexion angle by about 2°. To maintain the intended posture, the user may need to exert less physical effort than that predicted by Equation (2), probably due to the exoskeleton weight. Finally, the maximum displacement of the back frame is less than one millimeter, so the exoskeleton's normal operation should not be compromised (Figure 9b).

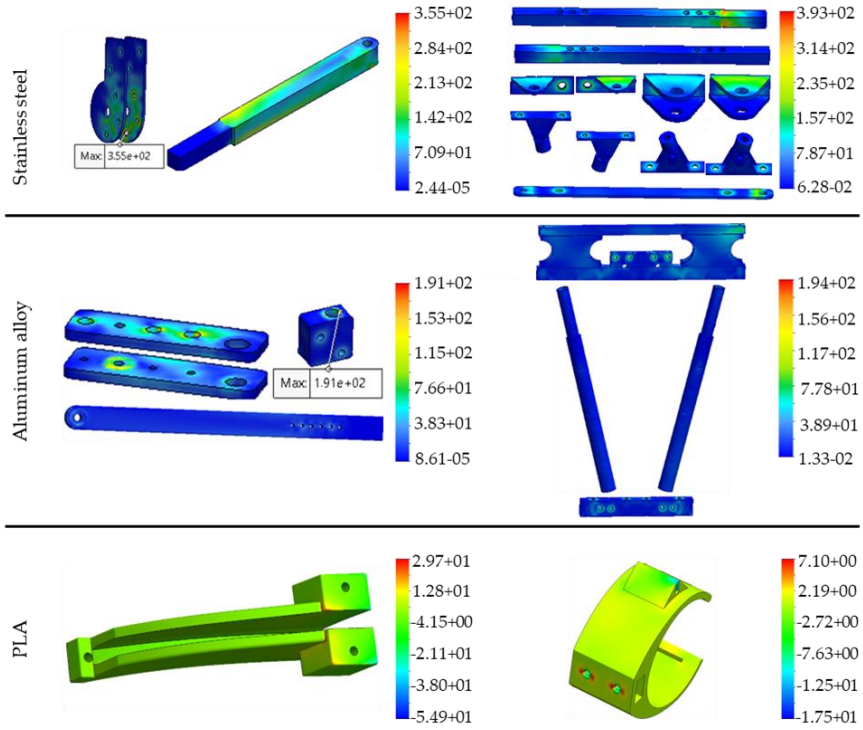

Figure 8. Von Mises stresses in stainless steel and aluminum components and maximum normal stress in the fiber direction of the PLA components. All stresses are in MPa.

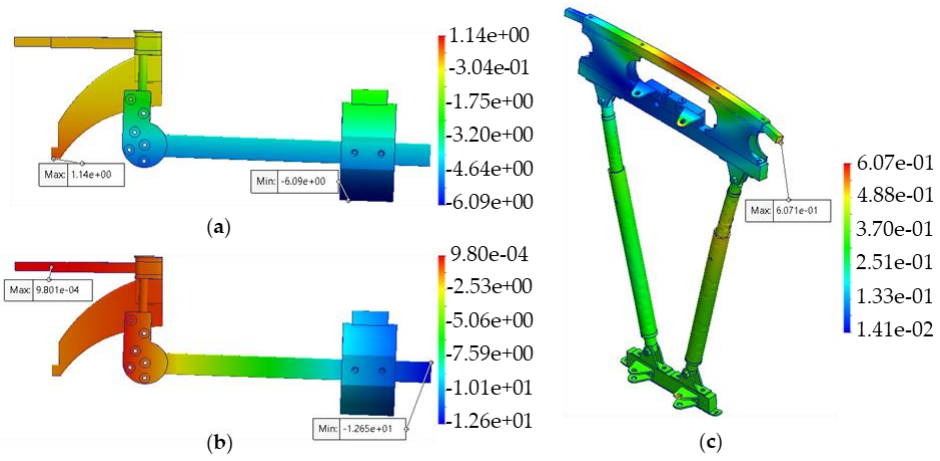

Figure 9. Displacements in the mechanical structure: (**a**) displacement in the anteroposterior direction of the exo-arm; (**b**) displacement in the cranio-caudal direction of the exo-arm; (**c**) displacement magnitude of the back frame represented with a scale of 20. All data are in mm.

The findings of the FEM study suggest that the designed exoskeleton provides steady support. As a result, the prototype illustrated in Figure 1 was built utilizing materials determined by FEM analysis. The overall weight of the exoskeleton prototype is around 5.5 kg, which is almost double that of existing devices on the market. However, it is important to remember that this is a prototype. In the future, the device's weight should be reduced by reshaping the exoskeleton components to optimize their stiffness-to-weight ratio and adopting lightweight, high-strength materials like carbon fiber whose usage in similar wearable systems has been already proven in several studies [26–28].

4.2. Experimental Test Results

In the static task (Figure 10a,b), the ARV of the anterior and middle deltoids decreases by about 66% and 55% in the loaded condition (right arm) and by about 64% and 45% in the unloaded condition (left arm). The percentage reductions in the anterior deltoid are higher than those reported for comparable exoskeletons (55% with PAEXO [11], 20% with MATE [20], and 57% with H-VEX [15]). Due to different arm postures induced by the exoskeleton, the activity of the medial deltoid is reduced by less than that of the anterior deltoid. As highlighted by the data listed in Table 3, the exoskeleton does not affect shoulder flexion but increases shoulder abduction. Since the middle deltoid muscle is responsible for shoulder horizontal abduction, altering arm posture may necessitate increasing medial deltoid muscular activity, which would lessen the beneficial effects on this muscle. However, the abduction of the arm caused by an exoskeleton has also been documented in earlier research [11,16].

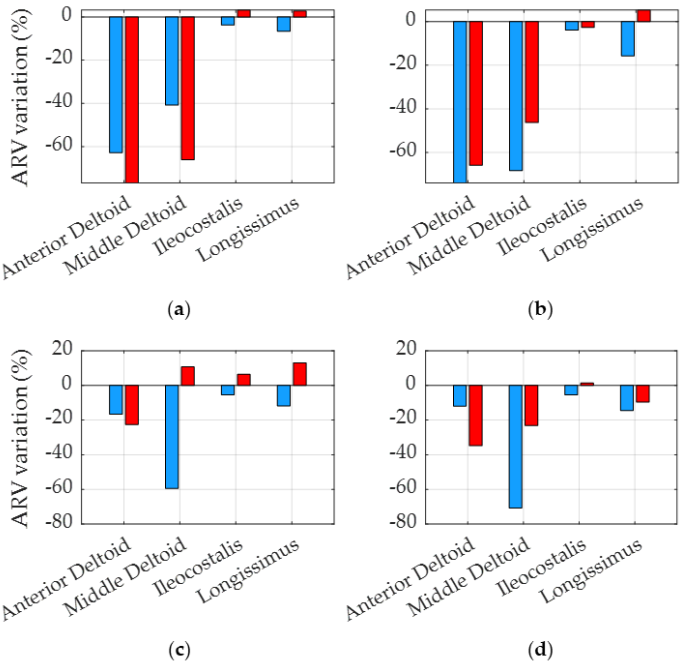

Figure 10. Muscles' ARV percentage variation between FREE and EXO trials of subject 1 (blue bars) and subject 2 (red bars): (**a**) static task of the left arm; (**b**) static task of the right arm; (**c**) dynamic task without tool; (**d**) dynamic task with tool. Negative values indicate decreased muscular activity in the EXO sessions.

In dynamic tests, abduction, flexion, adduction, and extension of the shoulder were performed in that order. Table 3 shows the width of the movements of the arm. During the dynamic tasks (Figure 10c,d), the ARV of the anterior and middle deltoid decreases by about 20% and 24% in the unloaded condition and by about 23% and 47% in the loaded condition. The decrease in muscle activity of the anterior deltoid is reduced with respect to static tasks. It should be considered that the flexion and horizontal adduction of the shoulder

are both attributed to the anterior deltoid. As a result, its muscular effort diminishes during the flexion movement due to the exoskeleton's support torque but increases during adduction since it counteracts the exoskeleton's activity. For the same reasons, the slightly increased middle deltoid activity registered in the tool-less test performed by subject 2 can be attributed to the broader abduction–adduction motions performed during the EXO session (see Table 3).

Table 3. Upper arm workspace during experimental tests.

Subject	Task	Tool	Shoulder Angle	FREE (°)	EXO (°)
1	Static	Yes	Flexion	78.8 ± 1.5	79.8 ± 0.4
			Abduction	9.9 ± 1.1	5.3 ± 0.4
		No	Flexion	83.3 ± 0.9	81.6 ± 0.6
			Abduction	2.3 ± 0.7	5.5 ± 0.3
	Dynamic	Yes	Abduction	12.7 ± 1.1	16.1 ± 1.4
			Flexion	15.4 ± 1.7	20.7 ± 3.0
			Adduction	11.8 ± 0.8	17.5 ± 1.8
			Extension	17.8 ±1.4	19.2 ± 1.7
		No	Abduction	13.5 ± 1.3	16.7 ± 1.4
			Flexion	18.3 ± 0.7	22.0 ±2.9
			Adduction	12.1 ± 1.0	17.4 ± 1.0
			Extension	18.2 ± 2.1	21.6 ± 2.4
2	Static	Yes	Flexion	85.2 ± 0.7	87.7 ± 0.4
			Abduction	5.5 ± 0.4	7.4 ± 0.3
		No	Flexion	90.4 ± 0.5	88.9 ± 0.2
			Abduction	2.5 ± 0.3	6.0 ± 0.1
	Dynamic	Yes	Abduction	8.5 ± 5.5	16.2 ± 3.5
			Flexion	25.6 ± 4.7	32.2 ± 2.5
			Adduction	13.5 ±2.7	19.5 ± 2.4
			Extension	29.1 ± 3.6	34.3 ± 2.8
		No	Abduction	16.0 ± 3.7	26.6 ± 2.7
			Flexion	36.8 ± 7.6	39.3 ± 1.1
			Adduction	16.9 ± 3.0	29.8 ± 2.9
			Extension	40.4 ± 4.5	42.4 ± 3.7

Generally, the exoskeleton relieves the physical strain on the primary shoulder elevator muscles. Furthermore, its support action is independent of the instrument held in the hand. Therefore, the support torque may be tailored to the specific working task by appropriately setting the MKM supply pressure. For the user, lowering muscular activity provides significant advantages. In the glenohumeral joint, the contraction of shoulder muscles produces intra-articular compression forces correlated with musculoskeletal disease incidence [29,30]. In addition, decreased muscular activity postpones the onset of muscle fatigue, which may cause shoulder impingement syndrome [31]. In light of the foregoing, the proposed exoskeleton could lower the risk of upper-limb work-related musculoskeletal illnesses. However, to verify the possible long-term advantages, additional research is necessary.

Industrial exoskeletons for upper limbs must not neglect wearability and portability because they cannot be attached to platforms to achieve the largest freedom of movement for the user. As a result, the upper limbs' support action comes at the cost of increased load in body parts that are more suitable to support loads, like the spinal joint and pelvis. Despite this, there is no discernible increase in the lumbar region muscular effort (Figure 10). In contrast, CoP_{rms} increases (Figure 11), demonstrating a balance performance reduction. Nevertheless, this negative effect can disappear by reducing the device's total weight [11]. A training session that helps the user to adjust to the increased weight may also improve postural function. Therefore, a training phase should be added in future investigations before the experimental test to help users become more familiar with the exoskeleton.

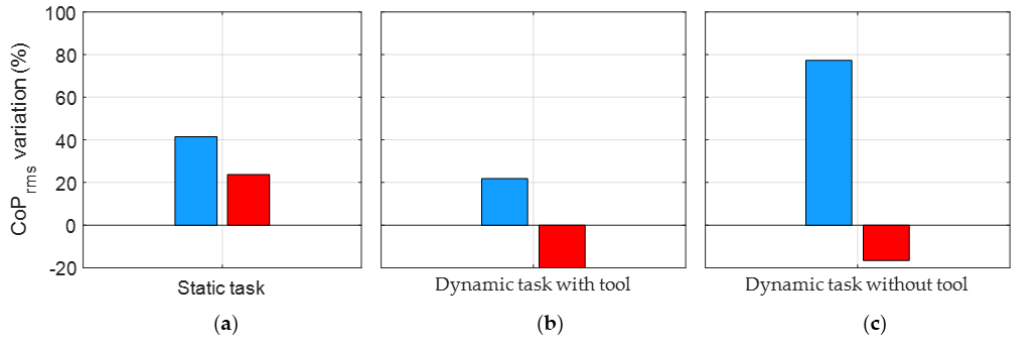

Figure 11. CoP_{rms} percentage variation between FREE and EXO trials of subject 1 (blue bars) and subject 2 (red bars): (**a**) static task; (**b**) dynamic task with tool; (**c**) dynamic task without tool. Positive values indicate increased CoP displacement in EXO sessions.

The following limitations should be taken into account when interpreting the experimental study's results: The sample was small and not representative of exoskeleton end-users. A larger sample size, including skilled manual handling workers, should be involved in future studies. A second limitation could be the features of the working scenarios simulated in static and dynamic trials during experimentation. The gestures and timing to which workers were exposed during the shift could be quite different from those tested in this study. In this sense, further testing of the exoskeleton for extended trial durations and tasks more typical of the job activities is also required. Moreover, dynamic tasks should be repeated at various rates to verify that the MKM's reaction time is sufficient to guarantee the assistance level regardless of movement speed. Lastly, the exoskeleton's impact on peripheral movements (e.g., walking, trunk rotation, and arm lowering) should be investigated.

5. Conclusions

A passive exoskeleton based on McKibben artificial muscles was developed for workers who must keep their arms in an elevated position for long periods. The results of the analytical model and the finite element analysis demonstrate that the designed exoskeleton is safe for the users. The contact pressures applied on the human tissue are low enough to prevent tissue injury or discomfort, and the structure can provide stable support for the arm.

A prototype was constructed, with the entire mass weighing 5.5 kg. The static and dynamic tasks suggested that the designed exoskeleton can alleviate shoulder load without overloading the lumbar area. On the other hand, the arms' range of movement is limited, although it remains sufficient to carry out a large number of working activities.

In the future, more extensive and comprehensive experimental tests will be needed to confirm the obtained results.

Author Contributions: Conceptualization, C.D.B., C.F. and M.P.; methodology, C.D.B., C.F. and M.P.; software, M.P.; validation, C.D.B. and M.P.; formal analysis, M.P.; investigation, C.D.B. and M.P.; writing—original draft preparation, C.D.B. and M.P.; writing—review and editing, C.F.; visualization, C.D.B. and M.P.; supervision, C.F. All authors have read and agreed to the published version of the manuscript.

Funding: This research received no external funding.

Data Availability Statement: The dataset is available upon request from the authors.

Conflicts of Interest: The authors declare no conflicts of interest.

References

1. Bai, S.; Christensen, S.; Islam, M.R.U. An Upper-Body Exoskeleton with a Novel Shoulder Mechanism for Assistive Applications. In Proceedings of the 2017 IEEE International Conference on Advanced Intelligent Mechatronics (AIM), Munich, Germany, 3–7 July 2017; pp. 1041–1046.

2. Ebrahimi, A. Stuttgart Exo-Jacket: An Exoskeleton for Industrial Upper Body Applications. In Proceedings of the 2017 10th International Conference on Human System Interactions (HSI), Ulsan, Republic of Korea, 17–19 July 2017; pp. 258–263.
3. Mauri, A.; Lettori, J.; Fusi, G.; Fausti, D.; Mor, M.; Braghin, F.; Legnani, G.; Roveda, L. Mechanical and Control Design of an Industrial Exoskeleton for Advanced Human Empowering in Heavy Parts Manipulation Tasks. *Robotics* **2019**, *8*, 65. [CrossRef]
4. Otten, B.M.; Weidner, R.; Argubi-Wollesen, A. Evaluation of a Novel Active Exoskeleton for Tasks at or Above Head Level. *IEEE Robot. Autom. Lett.* **2018**, *3*, 2408–2415. [CrossRef]
5. Maurice, P.; Camernik, J.; Gorjan, D.; Schirrmeister, B.; Bornmann, J.; Tagliapietra, L.; Latella, C.; Pucci, D.; Fritzsche, L.; Ivaldi, S.; et al. Objective and Subjective Effects of a Passive Exoskeleton on Overhead Work. *IEEE Trans. Neural Syst. Rehabil. Eng.* **2020**, *28*, 152–164. [CrossRef] [PubMed]
6. Wang, H.-M.; Le, D.K.L.; Lin, W.-C. Evaluation of a Passive Upper-Limb Exoskeleton Applied to Assist Farming Activities in Fruit Orchards. *Appl. Sci.* **2021**, *11*, 757. [CrossRef]
7. De Vries, A.; Murphy, M.; Könemann, R.; Kingma, I.; De Looze, M. The Amount of Support Provided by a Passive Arm Support Exoskeleton in a Range of Elevated Arm Postures. *IISE Trans. Occup. Ergon. Hum. Factors* **2019**, *7*, 311–321. [CrossRef]
8. Kozinc, Ž.; Babič, J.; Šarabon, N. Human Pressure Tolerance and Effects of Different Padding Materials with Implications for Development of Exoskeletons and Similar Devices. *Appl. Ergon.* **2021**, *93*, 103379. [CrossRef] [PubMed]
9. Graven-Nielsen, T.; Vaegter, H.B.; Finocchietti, S.; Handberg, G.; Arendt-Nielsen, L. Assessment of Musculoskeletal Pain Sensitivity and Temporal Summation by Cuff Pressure Algometry: A Reliability Study. *Pain* **2015**, *156*, 2193–2202. [CrossRef] [PubMed]
10. Kim, S.; Nussbaum, M.A.; Mokhlespour Esfahani, M.I.; Alemi, M.M.; Jia, B.; Rashedi, E. Assessing the Influence of a Passive, Upper Extremity Exoskeletal Vest for Tasks Requiring Arm Elevation: Part II—"Unexpected" Effects on Shoulder Motion, Balance, and Spine Loading. *Appl. Ergon.* **2018**, *70*, 323–330. [CrossRef] [PubMed]
11. Maurice, P.; Čamernik, J.; Gorjan, D.; Schirrmeister, B.; Bornmann, J.; Tagliapietra, L.; Latella, C.; Pucci, D.; Fritzsche, L.; Ivaldi, S.; et al. Evaluation of PAEXO, a Novel Passive Exoskeleton for Overhead Work. *Comput. Methods Biomech. Biomed. Eng.* **2019**, *22*, S448–S450. [CrossRef]
12. Kim, S.; Nussbaum, M.A.; Mokhlespour Esfahani, M.I.; Alemi, M.M.; Alabdulkarim, S.; Rashedi, E. Assessing the Influence of a Passive, Upper Extremity Exoskeletal Vest for Tasks Requiring Arm Elevation: Part I—"Expected" Effects on Discomfort, Shoulder Muscle Activity, and Work Task Performance. *Appl. Ergon.* **2018**, *70*, 315–322. [CrossRef]
13. Du, Z.; Yan, Z.; Huang, T.; Bai, O.; Huang, Q.; Zhang, T.; Han, B. Development and Experimental Validation of a Passive Exoskeletal Vest. *IEEE Trans. Neural Syst. Rehabil. Eng.* **2022**, *30*, 1941–1950. [CrossRef] [PubMed]
14. Yin, P.; Yang, L.; Qu, S.; Wang, C. Effects of a Passive Upper Extremity Exoskeleton for Overhead Tasks. *J. Electromyogr. Kinesiol.* **2020**, *55*, 102478. [CrossRef] [PubMed]
15. Hyun, D.J.; Bae, K.; Kim, K.; Nam, S.; Lee, D. A Light-Weight Passive Upper Arm Assistive Exoskeleton Based on Multi-Linkage Spring-Energy Dissipation Mechanism for Overhead Tasks. *Robot. Auton. Syst.* **2019**, *122*, 103309. [CrossRef]
16. Spada, S.; Ghibaudo, L.; Gilotta, S.; Gastaldi, L.; Cavatorta, M.P. Investigation into the Applicability of a Passive Upper-Limb Exoskeleton in Automotive Industry. *Procedia Manuf.* **2017**, *11*, 1255–1262. [CrossRef]
17. Bosch, T.; Van Eck, J.; Knitel, K.; De Looze, M. The Effects of a Passive Exoskeleton on Muscle Activity, Discomfort and Endurance Time in Forward Bending Work. *Appl. Ergon.* **2016**, *54*, 212–217. [CrossRef]
18. Theurel, J.; Desbrosses, K.; Roux, T.; Savescu, A. Physiological Consequences of Using an Upper Limb Exoskeleton during Manual Handling Tasks. *Appl. Ergon.* **2018**, *67*, 211–217. [CrossRef] [PubMed]
19. Sylla, N.; Bonnet, V.; Colledani, F.; Fraisse, P. Ergonomic Contribution of ABLE Exoskeleton in Automotive Industry. *Int. J. Ind. Ergon.* **2014**, *44*, 475–481. [CrossRef]
20. Pacifico, I.; Scano, A.; Guanziroli, E.; Moise, M.; Morelli, L.; Chiavenna, A.; Romo, D.; Spada, S.; Colombina, G.; Molteni, F.; et al. An Experimental Evaluation of the Proto-MATE: A Novel Ergonomic Upper-Limb Exoskeleton to Reduce Workers' Physical Strain. *IEEE Robot. Automat. Mag.* **2020**, *27*, 54–65. [CrossRef]
21. Huysamen, K.; Bosch, T.; De Looze, M.; Stadler, K.S.; Graf, E.; O'Sullivan, L.W. Evaluation of a Passive Exoskeleton for Static Upper Limb Activities. *Appl. Ergon.* **2018**, *70*, 148–155. [CrossRef]
22. Paterna, M.; Magnetti Gisolo, S.; De Benedictis, C.; Muscolo, G.G.; Ferraresi, C. A Passive Upper-Limb Exoskeleton for Industrial Application Based on Pneumatic Artificial Muscles. *Mech. Sci.* **2022**, *13*, 387–398. [CrossRef]
23. Magnetti Gisolo, S.; Muscolo, G.G.; Paterna, M.; De Benedictis, C.; Ferraresi, C. Feasibility Study of a Passive Pneumatic Exoskeleton for Upper Limbs Based on a McKibben Artificial Muscle. In *Advances in Service and Industrial Robotics*; Zeghloul, S., Laribi, M.A., Sandoval, J., Eds.; Mechanisms and Machine Science; Springer International Publishing: Cham, Switzerland, 2021; Volume 102, pp. 208–217, ISBN 978-3-030-75258-3.
24. Winter, D.A. *Biomechanics and Motor Control of Human Movement*, 4th ed.; Wiley: Hoboken, NJ, USA, 2009; ISBN 978-0-470-39818-0.
25. Hermens, H.J.; Freriks, B. *SENIAM 5. The State of the Art on Sensors and Sensor Placement Procedures for Surface ElectroMyoGraphy: A Proposal for Sensor Placement Procedures*; Roessingh Research and Development: Enschede, The Netherlands, 1997.
26. Zhao, L.; Yang, T.; Yang, Y.; Yu, P. A Wearable Upper Limb Exoskeleton for Intuitive Teleoperation of Anthropomorphic Manipulators. *Machines* **2023**, *11*, 441. [CrossRef]
27. Palazzi, E.; Luzi, L.; Dimo, E.; Meneghetti, M.; Vicario, R.; Luzia, R.F.; Vertechy, R.; Calanca, A. An Affordable Upper-Limb Exoskeleton Concept for Rehabilitation Applications. *Technologies* **2022**, *10*, 22. [CrossRef]

28. Zeiaee, A.; Zarrin, R.S.; Eib, A.; Langari, R.; Tafreshi, R. CLEVERarm: A Lightweight and Compact Exoskeleton for Upper-Limb Rehabilitation. *IEEE Robot. Autom. Lett.* **2022**, *7*, 1880–1887. [CrossRef]
29. European Agency for Safety and Health at Work; IKEI; Panteia. *Work-Related Musculoskeletal Disorders: Prevalence, Costs and Demographics in the EU*; Publications Office: Luxembourg, 2019.
30. Grieve, J.R.; Dickerson, C.R. Overhead Work: Identification of Evidence-Based Exposure Guidelines. *Occup. Ergon.* **2008**, *8*, 53–66. [CrossRef]
31. Hall, S.J. *Basic Biomechanics*, 6th ed.; McGraw-Hill: New York, NY, USA, 2012; ISBN 978-0-07-337644-8.